PAPER

Check for updates

Systematic investigation of the influence of electronic substituents on dinuclear gold(I) amidinates: synthesis, characterisation and photoluminescence studies†

Frederic Krätschmer,[a] Xin Gui,[b] Michael T. Gamer, [ID][a] Wim Klopper [ID][b] and Peter W. Roesky [ID] *[a]

Dinuclear gold(I) compounds are of great interest due to their aurophilic interactions that influence their photophysical properties. Herein, we showcase that gold–gold interactions can be influenced by tuning the electronic properties of the ligands. Therefore, various *para* substituted (R) *N,N′*-bis(2,6-dimethylphenyl)formamidinate ligands (*p*RXylForm; Xyl = 2,6-dimethylphenyl and Form = formamidinate) were treated with Au(tht)Cl (tht = tetrahydrothiophene) to give *via* salt metathesis the corresponding gold(I) compounds [*p*RXylForm$_2$Au$_2$] (R = −OMe, −Me, −Ph, −H, −SMe, and −CO$_2$Me). All complexes showed intense luminescence properties at low temperatures. Alignment with the Hammett parameter σ_p revealed the trends in the ^{1}H and ^{13}C NMR spectra. These results showed the influence of the donor–acceptor abilities of different substituents on the ligand system which were confirmed with calculated orbital energies. Photophysical investigations showed their lifetimes in the millisecond range indicating phosphorescence processes and revealed a redshift with the decreasing donor ability of the substituents in the solid state.

Introduction

Due to its applications in various fields such as catalysis, medicine and small molecule activation, increasing research on molecular gold(I) compounds has been observed during the last few decades.[1] In particular, dinuclear gold(I) complexes have been investigated in terms of their photophysical properties, which are influenced in many cases by aurophilic interactions.[2–7] The concept of "aurophilic interactions" or "aurophilicity" was established by H. Schmidbaur in 1989 and describes the attractive interactions of gold cations.[8,9] These attractive forces between cations, which are at first glance counter-intuitive, have been the subject of intensive theoretical investigations. Pyykkö showed by theoretical methods that aurophilicity is mainly a consequence of dispersion forces and is enhanced by relativistic effects.[10] Although discussions about the concept are still ongoing,[11–15] this interpretation has been widely accepted.[16–21] Nowadays, it is common knowledge that

such attractive forces are not only limited to gold cations but also observed in compounds containing other heavy-metal closed-shell cations.[22,23] Thus, aurophilicity is just a special case of so-called metallophilicity. In addition, argentophilic and mercurophilic interactions have been observed and described.[24,25] In general, aurophilic interactions are likely to exist if the distance of two gold atoms is below 3.5 Å, although the respective van der Waals distance (3.32 Å) is shorter.[5,20,26,27] The binding energy of these interactions may reach values of up to 50 kJ mol^{-1}, which can be divided into three cases: fully-supported (**I**), semi-supported (**II**) and unsupported (**III**) (Fig. 1).[28,29] In comparison with mononuclear gold(I) compounds, different photophysical properties were observed in the presence of Au···Au[28] or Au(I)···M interactions (M = heavy atom).[30,31] The excited state of complexes with aurophilic Au···Au contacts has been suggested to be due to ligand-to-metal–metal charge-transfer (LMMCT).[32–34]
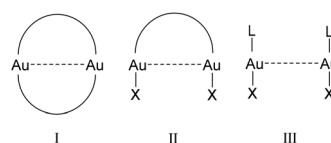
[a]Institute of Inorganic Chemistry, Karlsruhe Institute of Technology, Engesserstr. 15, 76131 Karlsruhe, Germany. E-mail: roesky@kit.edu
[b]Institute of Physical Chemistry, Karlsruhe Institute of Technology, Fritz-Haber-Weg 2, 76131 Karlsruhe, Germany
†Electronic supplementary information (ESI) available. CCDC 2120940–2120944. For ESI and crystallographic data in CIF or other electronic format see DOI: 10.1039/d1dt03795a

Fig. 1 Classification of closed-shell aurophilic interactions into fully-supported (**I**), semi-supported (**II**) and unsupported (**III**).

An established method for the synthesis of dinuclear gold(I) complexes featuring "fully supported" aurophilic interactions is the employment of amidinate ligands.[35–37] Following the synthesis of the first gold(I) bis(amidinate) complex by Dehnicke and co-workers,[38] this field was expanded to the synthesis of several other bis(amidinate) gold(I) compounds.[39–42] Pioneering work on the reactivity of dinuclear gold(I) amidinate compounds towards small molecules was carried out by Fackler et al. They investigated the oxidative addition of small molecules (e.g., Cl_2, Br_2, and I_2) to the dinuclear gold(I) complex $[Au_2(2,6-Me_2-Form)_2]$, which resulted in the formation of complexes with an Au(II)···Au(II) bond, with the most stable and most commonly found Au_2^{4+} core.[6,43–45]

Another possibility to enhance the properties of dinuclear gold(I) complexes is the functionalisation of the NCN backbone. Previously, our group reported the photophysical properties of acetylide functionalised gold(I) complexes and the investigation of multinuclear coinage metal compounds.[46–50]

In general, amidinate ligands are available with a large variety of substituents. By using para-phenyl substituents on the nitrogen atom, the electronic properties of the resulting ligands can be selectively tuned without changing the steric demand.[51] In light of these properties, we faced the challenge to synthesise various dinuclear gold(I) compounds, which are ligated by amidinate ligands having different electronic properties (Scheme 1). As a scale for the intensity of the electronic influence, the Hammett parameter was applied.[52,53] Similar studies have been reported by Tunik et al., who investigated the influence of the ligand substituents of gold–copper alkynyl complexes on their photoluminescence properties. Using the Hammett parameter as the reference, they were able to reveal a substantial redshift of the emission maxima with the increase in the electron-donating properties of the ligands.[54]

Herein, we report the synthesis of six different dinuclear gold complexes exhibiting fully supported aurophilic interactions by using a variety of formamidinate ligands with different substituents in para position on the 2,6-dimethylphenyl side groups. All complexes were fully characterised by SCXRD, multinuclear NMR spectroscopy, IR spectroscopy, ESI mass spectrometry, elemental analysis and photoluminescence experiments. In addition, theoretical studies regarding the influence of the respective substituents on the supported aurophilic interactions and luminescence properties were performed at the GW approximation and Bethe–Salpeter equation (GW/BSE) level.
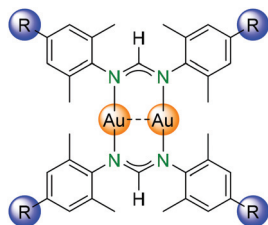

Scheme 1 Target complexes in which the amidinate ligands have different electronic properties but a similar steric demand upon coordination.

Results and discussion

Synthesis and characterisation

The setup of the ligand framework is shown in Scheme 1. As a substituent of the nitrogen atoms, we used 2,6-xylidine (2,6-dimethylphenyl) as the basic scaffold and added different substituents (Scheme 2) at the para-position. By using this setup, we generated ligands with essentially the same steric demand upon coordination. The differently substituted amidine ligands L^1–L^6 were synthesised by an ethanol condensation reaction from the corresponding amines and triethyl orthoformate (Scheme 2).[55–64]

While most of the reagents for the ligand synthesis are commercially available, the amine precursors for L^1, L^3 and L^5 were synthesised according to literature-known procedures.[59,62,63] In the case of L^3, 4-phenyl-xylidine was obtained by the literature-known Suzuki coupling reaction of 4-bromo-xylidine with phenylboronic acid, followed by amidine condensation.[64] We also established a second route for obtaining this ligand by synthesising N,N′-bis(4-bromo-2,6-dimethylphenyl)formamidine first,[57] followed by cross coupling under similar conditions (Scheme 3). The advantage is the
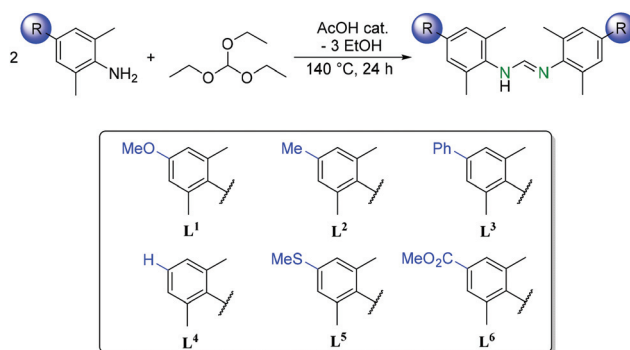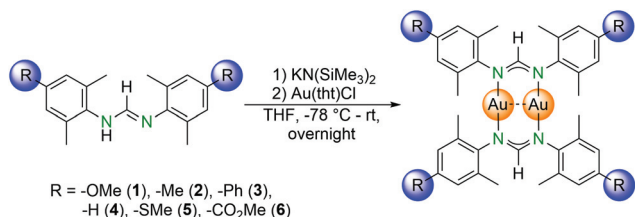

Scheme 2 Synthesis of amidine ligands L^1–L^6 via the ethanol condensation reaction.
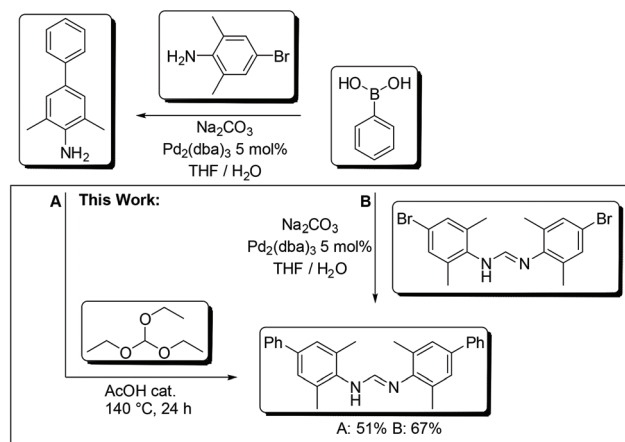
Scheme 3 Synthesis routes of L^3 with Suzuki coupling before (left) and after (right) amidine formation.

R = -OMe (**1**), -Me (**2**), -Ph (**3**),
-H (**4**), -SMe (**5**), -CO₂Me (**6**)

Scheme 4 Synthesis of gold complexes **1–6**.

significantly better separation through column chromatography of the cross-coupling product. In the end, we were able to synthesise and fully characterise the new amidine ligands L^3, L^5 and L^6.

Depending on the solvent used, the obtained ^{1}H NMR spectra of L^1–L^6 show complex resonances due to E/Z isomerisation and tautomerisation.[51] Ligands L^1, L^4 and L^6 exist as two isomers in a 2 : 3 ratio when measured in C_6D_6, showing a pattern of three singlets in a 1 : 3 : 1 ratio for the 2,6-methyl protons, while L^2 and L^3 exist in a 1 : 1 ratio with a 1 : 2 : 1 pattern. The two small singlets belong to the 2,6-methyl protons of the E-isomer and the large singlet to the Z-isomer. These patterns were also found for the phenyl protons of L^1, L^2, L^4 and L^6 in the ^{1}H NMR and ^{13}C{^{1}H} NMR spectra (see the ESI Fig. S1–S6, S11 and S12†). In addition, two signals were observed for the NH proton, one at around 5 ppm and the other downfield shifted at around 7 ppm. In the ^{13}C{^{1}H} NMR spectra, the NCN carbon resonances appear between 140 and 150 ppm for all ligands. The N–H stretching mode occurs in the typical range at around 3200 cm^{-1} in the IR spectra (ESI Fig. S35–S40†).[51]

Subsequently, the bis(amidinate) gold(I) complexes **1–6** were synthesised via salt elimination from the in situ generated potassium salt of ligands L^1–L^6 and Au(tht)Cl in THF (Scheme 4).

Compounds [pRXylForm₂Au₂] R = −OMe (**1**), −Me (**2**), −Ph (**3**), −SMe (**5**) and −CO₂Me (**6**) were crystallised by slow evaporation of THF (**1–3** and **5**) or toluene (**6**), while single crystals of [XylForm₂Au₂] (**4**) were obtained by a literature known procedure (Fig. 2).[44] The complexes were obtained in good yields between 40% and 68%. Complete deprotonation of the ligands was confirmed by the disappearance of the N–H band in the IR spectra (ESI Fig. S41–S46†) and the corresponding N–H resonance in the ^{1}H NMR spectra (ESI Fig. S13–S26†). The complexes are stable in the solid state under an inert atmosphere and exclusion of light for several months, but in solution, decomposition occurs within a few days. Compounds **1**, **4** and **6** crystallise in the triclinic space group $P\bar{1}$, **2** in the monoclinic space group $C2/c$, **3** in $P2_1/c$ and **5** in the trigonal space group $R\bar{3}c$. The Au⋯Au distances range from 2.7079(7) Å in **1** to 2.7366(2) Å in **3** (Fig. 2). These compounds show similar Au⋯Au distances as reported in the literature for other bimetallic gold amidinate complexes, for example [{(Me₃SiC≡CC(NDipp)₂)₂Au₂] (2.7009(11) Å).[46] The smallest amidinate bite angle (126.7(3)°) is seen for compound **1** and the largest for **4** (128.5(9)°). These values

match well with the literature.[44,46] The Au–N bond lengths for each compound (approximately 2.03 Å) are in good agreement with those of other literature known gold amidinates. Moreover, the N–C1 bond lengths (ca. 1.30 Å), which are approximately the same in all complexes, fit well with those of some other related gold(I) amidinate complexes.[41,42,46] The twist angle (C₁–N$_x$–Ph; x = 1 and 2) of the phenyl rings of the amidinates differs for each compound. The phenyl rings of **2** and **4–6** are twisted conrotatory, with compounds **4** and **6** having the largest difference between their angles on each side (30° and 1°), while compounds **2** and **5** have almost an identical twist angle of around 10°. In contrast, the phenyl rings of compounds **1** and **3** are turning disrotatory, having one smaller and one larger angle; for example, **1** (4° and 11°) (Fig. 3).

Since the Au⋯Au distances are well below 3.5 Å, aurophilic interactions appear to exist in the sense of distance criterion, but one should be aware of the fact that we are dealing with fully supported aurophilic interactions. The short distance may very well result simply from the structural properties of the ligand. To investigate this in detail, we have performed Hartree–Fock calculations, which do not account for dispersion forces at all and post-Hartree–Fock calculations, which do account for dispersion (e.g., Møller–Plesset perturbation theory to the 2nd order, MP2, and spin-component-scaled MP2, SCS-MP2). Calculations were performed only for compound **4**. However, its silver(I) counterpart (**4-Ag**), was also studied, because the argentophilic interactions are usually much smaller than the aurophilic ones. Results for the relevant structural parameters are shown in Table 1.

It is clear from the computational results shown in Table 1 that in fully supported situations, the Au⋯Au distance criterion (<3.5 Å) is less suited to identify aurophilic interactions. The short distance is mainly a consequence of the ligand structure, i.e., the Au1–N1–C1 (cf. Table 1) and the N1–C1–N2 angles (between 127.0° and 128.5°). Very similar distances are found for Ag, although the dispersion forces should be much smaller than those for Au. From the viewpoint of the Hartree–Fock theory, it became clear that the electron-correlation effects are important (cf. SCS-MP2 and MP2 results), but they just lead to an overall shrinkage of the molecular structure. Nevertheless, Au⋯Au electronic interactions do exist and influence the photophysical properties. In the fully supported case, however, these interactions are enforced by the supporting ligands and should perhaps not be called "aurophilic interactions", since the latter is solely due to the London dispersion interactions between filled 5d^{10} shells.

Neither the electronic influence of the substituents seems to have a significant impact on Au⋯Au distances as shown in Table 2. The electronic properties of these substituents can be described by the Hammett parameter σ_p with –OMe (**1**) being the strongest electron-donating group and –CO₂Me (**6**) being the strongest electron withdrawing group. The Au⋯Au distances in the solid state structures are most likely influenced by the packing effects due to the steric demands of the substituents of the phenyl ring and cannot be ascribed to the electronic influence.
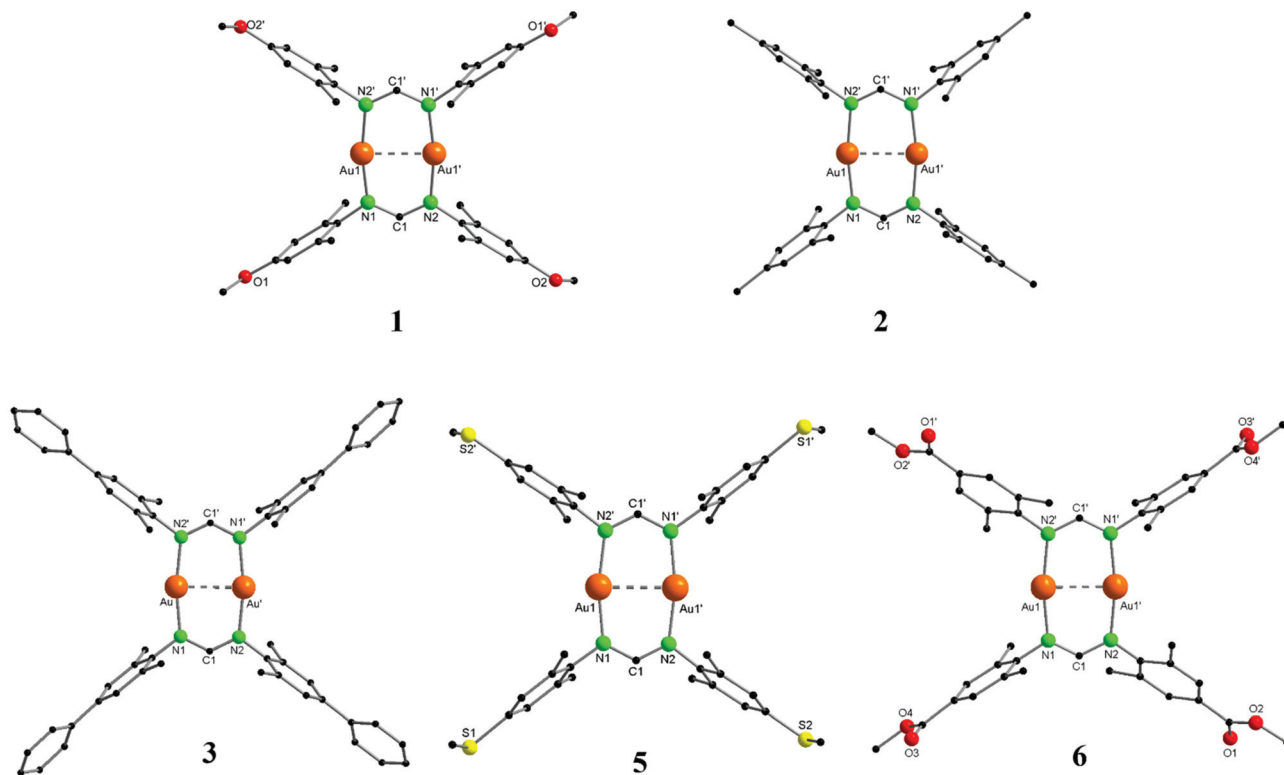
Fig. 2 Molecular structure of compounds **1–3**, **5** and **6** in the solid state. Hydrogen atoms and non-coordinating solvent molecules are omitted for clarity. Structural parameters are given in the ESI (Fig. S65–S69).†
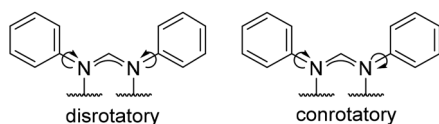
Fig. 3 Rotation of the phenyl rings to each other.

disrotatory   conrotatory

Table 1 Selected distances and angles of compound **4** and its silver(I) counterpart **4-Ag**, as obtained as various levels of computation

Distance	Method[a]	4	4-Ag
M1···M1′, M = Au, Ag (Å)	Hartree–Fock	2.852	294.5
	PBE0	2.759	2.770
	PBE0-D3(BJ)	2.752	2.763
	SCS-MP2[b]	2.738	2.777
	MP2[b]	2.702	2.743
M1···N1, M = Au, Ag (Å)	Hartree–Fock	2.102	2.208
	PBE0	2.044	2.101
	PBE0-D3(BJ)	2.039	2.096
	SCS-MP2[b]	2.009	2.061
	MP2[b]	1.988	2.030
∠M1–N1–C1, M = Au, Ag (°)	Hartree–Fock	122.6	124.6
	PBE0	121.4	122.3
	PBE0-D3(BJ)	121.5	122.3
	SCS-MP2[b]	121.5	122.8
	MP2[b]	121.3	122.5

[a] The basis set used is def2-TZVP. [b] In the frozen-core approximation.

Table 2 Hammett parameter σ_p for the substituents compared with the Au···Au distance of compounds **1–6**

	1	2	3
R	–OMe	–Me	–Ph
σ_p	−0.27	−0.17	−0.01
Au···Au	2.7079(7)	2.7277(4)	2.7366(2)

	4	5	6
R	–H	–SMe	–CO₂Me
σ_p	0.00	0.00	0.45
Au···Au	2.711(3)	2.7307(12)	2.7194(2)

In contrast to the ^{1}H NMR spectra of **L¹–L⁶**, well-defined signals are observed for **1–6**. Due to the deprotonation, all isomers are transformed into only one symmetric species, which coordinates to the gold atoms. It turned out that the N₂C(*H*) proton, which was detected in the range of 7.42 to 7.66 ppm, is a suitable probe for studying the electronic influence of the different substituents of the phenyl rings in the *para*-position on the ligand. Using the Hammett parameter, the signals for the proton in the backbone of compounds **1–6** can be lined up (except **3**) in a linear correlation according to the withdrawing and donating ability of their substituents, resulting in a shift of around 0.2 ppm (Fig. 4). This is related to the shielding of the proton by electron density, which is influenced by the substituents. The proton signal of com-
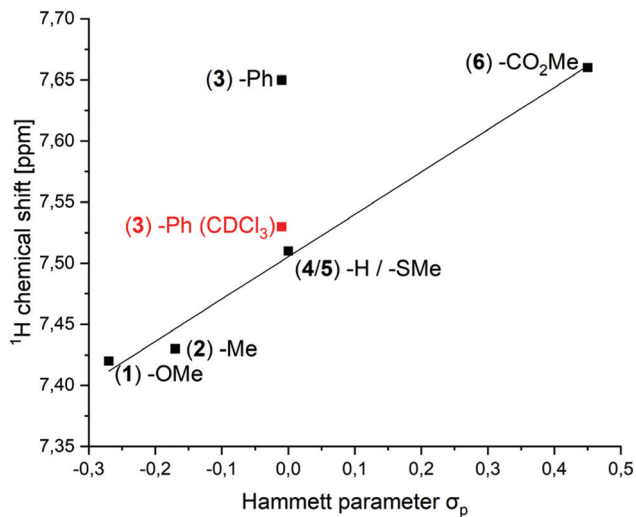
Fig. 4 Influence of the Hammett parameter σ_p of several substituents on the chemical shift of the $N_2C(H)$ proton of compounds **1–6** measured in THF-d_8.
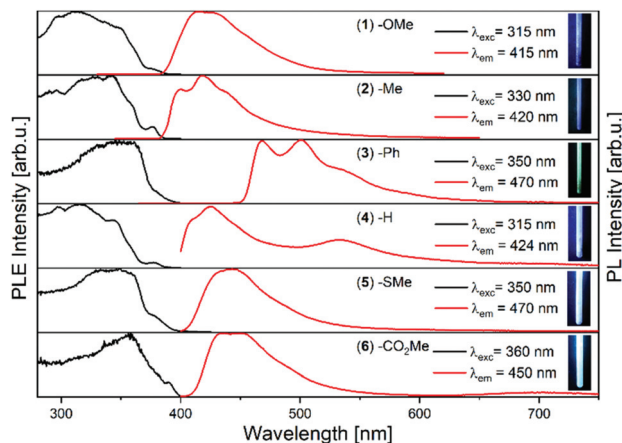

Fig. 5 Excitation and emission spectra of compounds **1–6** in the solid state at 77 K. The PLE/PL spectra were excited/recorded at the values given on the right side of the graph. Photographs of the PL samples: UV lamp (λ_{exc} = 256 nm).

pound **3** cannot be aligned with the others when measured in THF-d_8.

By changing the solvent to $CDCl_3$, a significant upfield shift from 7.66 ppm (THF-d_8) to 7.53 ppm ($CDCl_3$) is observed in the ^1H NMR spectrum of **3**. This leads to a conclusion that compared to the other complexes, compound **3** shows a different behaviour in THF solution. We suggest that this difference arises from the improved π-stacking interactions of the phenyl substituents in polar solvents.[65]

The N*C*N carbon atom of the ligand backbone is a sensitive probe for $^{13}C\{^1H\}$ NMR. Upon deprotonation of the ligand and coordination towards the gold centers, a strong downfield shift starting from around 140 ppm (N*C*NH) to about 170 ppm (N*C*N) was detected in the $^{13}C\{^1H\}$ NMR spectra. Compound **6** shows a slightly less shifted signal at around 169.5 ppm, while **1** shows the most significant downfield shifted resonance at 171.2 ppm. An opposite trend to that mentioned above for the ^1H shifts can be observed for the N*C*N carbon signals, where electron-donating groups lead to a downfield shift of around 1.7 ppm from **6** to **1** (see the ESI Fig. S27 (right)†).

Photoluminescence properties

We examined the luminescence properties of dinuclear gold(I) complexes **1–6** in the solid state and in frozen solution (THF) at 77 K. All compounds showed bright blue-green luminescence at low temperatures. UV-vis spectra were recorded for compounds **1–6** showing similar absorption with a band for **1**, **2** and **4** at 256 nm, which is redshifted for **3** (283 nm), **5** (272 nm) and **6** (260 nm). An additional band for compound **6** was detected at 288 nm (see the ESI† Fig. S47–S52). Note that the samples were measured in THF, and thus the band at 112 nm was referred to as the solvent.

In the photoluminescence emission (PL) and excitation (PLE) spectra, compounds **1–6** show broad absorption at low temperatures from UV (280 nm) up to 370 nm in the solid state and broad emission bands in the range from around 400 nm to 600 nm. Similar spectra were obtained for **1–2** and **4–6** in the solid state (Fig. 5). Only compound **3**, while strongly red-shifted, shows well-defined emission bands featuring the typical vibronic pattern of luminescent gold compounds.[66,67]
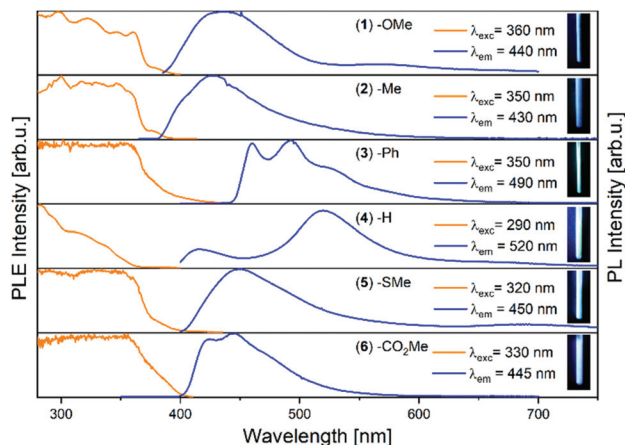
The spectra of compounds **1–6** (except **4**) in solution resemble the spectra in the solid state. For **4**, a decrease in absorption at 310 nm in solution is seen. Moreover, the emission maximum of **4** in the solid state is observed at 425 nm with a second smaller band at 523 nm, which is reversed in solution with the emission maximum at a longer wavelength (519 nm) (Fig. 6). A blueshift in the emission spectra of **1**, **3** and **4** can be observed from the solid state to solution, while those of **2**, **5** and **6** are red-shifted (Table 3).

Another major difference between the emission in the solid state and in solution is the appearance of weak bands at higher wavelengths for **1**, **5** and **6**. While **6** shows an additional weak band at 700 nm in the solid state, which is not visible in solution, **1** and **5** feature extra bands in solution (570 nm for **1** and 690 nm for **5**).

Table 3 shows a weak trend for λ_{max} in the emission spectra in the solid state. Upon increasing the electron withdrawing ability (increasing Hammett parameter σ_p), the maximum emission wavelength tends to increase due to the electronic influence of the substituents leading to a shift of 35 nm for **1** to **6**. This trend, however, is only observed in the solid state. In contrast to this, solvent effects overlay this weak trend. The largest difference can be seen for compound **4**, where the emission maximum is shifted by around 100 nm. Compound **3** cannot be aligned with the others. A strong redshift for the emission maximum was detected, presumably due to the abovementioned π-interaction also seen for the ^1H NMR signal of $N_2C(H)$ of compound **3** (Fig. 4).

Earlier, Tunik *et al.* reported an opposite result of the influence of the electronic properties represented by the Hammett

Fig. 6 Excitation and emission spectra of compounds **1–6** in frozen solution at 77 K. The PLE/PL spectra were excited/recorded at the values given on the right side of the graph. Photographs of the PL samples: UV lamp (λ_{exc} = 256 nm).

Table 3 Values of excitation and emission λ_{max} [nm] in the solid state and in THF at 77 K of compounds **1–6**

	1	**2**	**3**	**4**	**5**	**6**
λ_{max} exc, solid	313	343	349	316	350	358
λ_{max} em, solid	416	419	501	425	443	451
λ_{max} exc, THF	298	300	282	284	334	353
λ_{max} em, THF	437	429	492	519	449	446

parameter. They observed for gold–copper alkynyl complexes a bathochromic shift with the increase in donor ability.[54] However, their ligand system and metal atom scaffold differ significantly from our rather simple dinuclear gold(I) core and amidinate ligation. This leads to the conclusion that the impact of the electronic influence can be altered with the ligand system.

Compounds **1–6** show phosphorescence, measured at λ_{max}, with decay times that are in the range of microseconds from about 0.02 ms to 1.36 ms (see the ESI Fig. S34 and Table S1†). Most of the compounds feature complicated and unusual PL kinetics, meaning that their decay traces can only be well fitted by at least two exponential components. Compound **3** exhibits a particularly long phosphorescence lifetime of 1.36 ms in THF and 1.23 ms in the solid state.

Quantum chemical calculations

To further investigate the photophysical properties of the dinuclear gold(I) amidinate complexes with different modifications on the ligand, quantum chemical calculations were performed with the TURBOMOLE program package.[68] The ground-state equilibrium geometries were optimised at the PBE0-D3(BJ)/def2-TZVP level of theory,[69–72] showing good agreement with the experimental data for the bond lengths in the complex but a slight divergence for the angles of the substituted phenyls, and an overall elongation of the Au···Au inter-
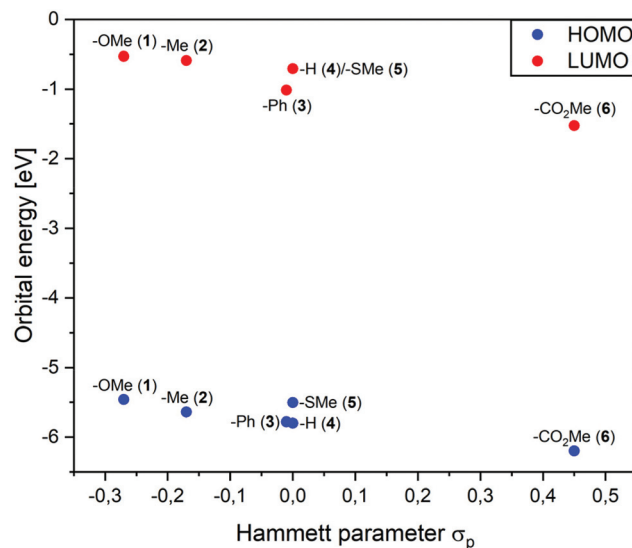
Fig. 7 Frontier orbital energies (eV) with respect to the Hammett parameter of the substituents.

action (Cartesian coordinates can be found in the ESI†). Excited-state calculations utilising the GW approximation and Bethe–Salpeter equation (GW/BSE)[73,74] were performed at the one-component (1c, scalar-relativistic) level for absorption spectra, and the quasirelativistic two-component (2c, including spin–orbit coupling) level for emission spectra. Computations were carried out for hypothetical complexes in addition to complexes **1–6** with dimethylamino (complex **7**), bromo (complex **8**) and nitro (complex **9**) substituents at the *para*-positions of the phenyl rings (see the ESI Fig. S70†).

The calculated frontier orbital energies of complexes **1–6** show a clear decreasing trend with the increasing electron-withdrawing ability of the substituents (Fig. 7). This trend still remains after taking the two extreme cases **7** and **9** into account (see the ESI Table S6†). Due to the similar drop in the HOMO and LUMO energies when bearing different substituents, the trend along the HOMO–LUMO gap of the gold complexes is rather weak, leading to only small differences in photoluminescence.

All complexes display metal-to-ligand charge-transfer (MLCT) absorption bands at around 240–270 nm (ESI† Fig. S71), which fit with the experimental UV-vis spectra (Fig. 8). The two alkyl-substituted complexes **2** and **4** exhibit very similar absorption profiles with the MLCT peak centred at 240 nm. The introduction of the electron-donating methoxy groups does not alter the absorption profile of complex **1**, resulting only in a slightly higher intensity of the MLCT peak. However, when the methoxy groups are replaced with methyl-thio groups, a significant redshift and increased intensity are observed in the predicted absorption spectrum of complex **5**. On the other hand, after introducing the electron withdrawing methoxycarbonyl groups, the predicted absorption spectrum of complex **6** features a significantly redshifted and broader MLCT absorption band. Interestingly, the phenyl substituted
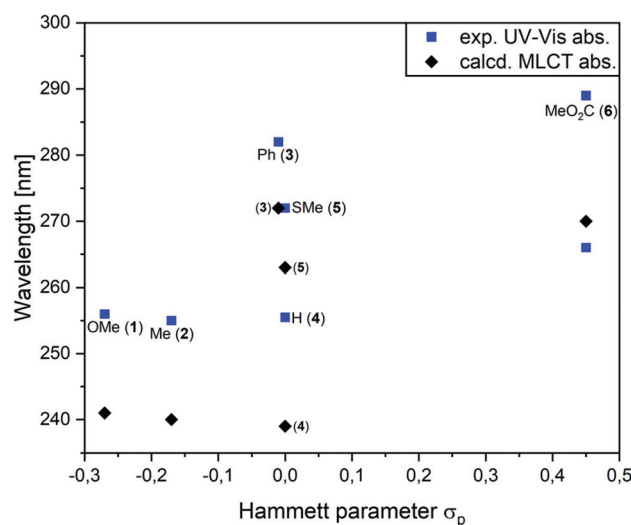
Fig. 8 Comparison of the experimental (blue) and calculated (black) UV-vis spectra.

Fig. 9 Emission maxima (nm) with respect to the Hammett parameter of the substituents.

complex **3** shows the most intense absorption peak. According to the unrelaxed difference density plots, the electron-donating and electron-withdrawing properties of the substituents are reflected in the change of electron density. However, the charge transfer from the gold centre to the aromatic groups of the amidinate ligands does not obviously differ and is actually quite similar among all the complexes.

The calculated emission maxima are in good agreement with the experimental data. The typical MLCT peak in the visible range is split into two distinct (shoulder) peaks, and the high-energy peak consists of one component of the most intense triplet excitation in the energetic range between S_1 and T_1, which starts to gain intensity from strong mixing with the singlet states. Natural transition orbital (NTO) analysis further confirms the MLCT character of the triplet excited states, and the NTOs are quite similar among all the complexes. Besides, all complexes turn out to present similar lifetimes in the range of tens or a few hundreds of microseconds, which also agree well with the experiment.

As shown in Fig. 9 and in Table S6,† with the increasing electron-withdrawing abilities of the substituents, the absorption spectra tend to redshift while the emission spectra tend to blueshift. Therefore, compared to the measured emission spectra in the solid state, the calculated gas-phase emission spectra exhibit an opposite trend with respect to the Hammett parameter. When the solvent effects are accounted for in the computations by means of the conductor-like screening model (COSMO, $\varepsilon = \infty$),[75] the trend is still opposite. Thus, solvent effects are not the reason for the opposite dependence on the Hammett parameter seen in the computations. Rather, we note that the frontier orbitals respond to the electron-donating and electron-withdrawing properties in a very similar manner (Fig. 7), leading to large uncertainties when computing the differences (*e.g.*, HOMO–LUMO gap).
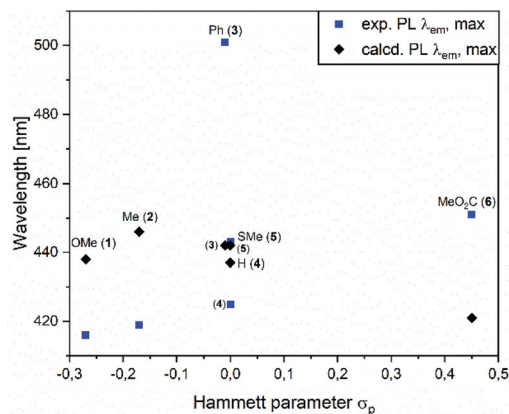
The different behaviour of compound **3** indicates the presence of some sort of π-interaction. Also, the shifted $\lambda_{\max}$ value of compound **4** from the solid state to solution arises most likely from solvent interactions.

For a detailed description of the computational methods, the calculated absorption and emission spectra, and a detailed analysis of the relevant excitation (including natural transition orbitals and unrelaxed difference density plots), we refer to the ESI.†

Summary

We presented the synthesis and characterisation of several dinuclear gold(I) complexes. These complexes were easily obtained by deprotonation of an amidine ligand *in situ* and addition to the gold precursor in THF. We further investigated the influence of the electronic groups attached at the *para* position of the side groups of the amidine ligands on the behaviour of the dinuclear gold(I) complexes. The influence of the different substituents resulted in changed NMR shifts and luminescence properties. With the increasing Hammett parameter, we observed a downfield shift of the signal of the proton in the formamidinate backbone ($N_2C(H)$ proton). Furthermore, a redshift of the emission bands was seen in the solid state. In both cases, only the phenyl-substituted compound does not fit in this trend, most probably due to the π-interactions.

Quantum chemical calculations showed a clear trend for the frontier orbital energies and a less obvious trend for the HOMO–LUMO gap energies. Further calculations showed an MLCT band fitting with the UV-vis spectra and good agreement of the emission maxima with the experimental data. An inverse trend was observed for the emission maxima in the luminescence spectra between the experimental solid state measurement and the calculated gas-phase spectra, which cannot be explained by the missing solvent and intermolecular interactions in the calculations. Geometry optimisation of all

compounds showed that the overall bonds are in good agreement, but the phenyl angles and Au···Au distances differ slightly from the experimental data.

Author contributions

The manuscript was written through the contributions of all authors. F. K. synthesised and analysed all presented compounds under the supervision of P. W. R. Solid state and solution PL analyses were conducted by F. K. and the data were interpreted by F. K. Theoretical investigations were performed by X. G. under the supervision of W. K. XRD data were refined by M. T. G. The original idea was from P. W. R. who supervised the work and interpreted the data. All authors have given approval to the final version of the manuscript.

Conflicts of interest

There are no conflicts to declare.

Acknowledgements

Notes and references

1 R. S. Ramon, N. Marion and S. P. Nolan, *Chem. – Eur. J.*, 2009, **15**, 8695–8697.
2 S. J. Freakley, Q. He, C. J. Kiely and G. J. Hutchings, *Catal. Lett.*, 2014, **145**, 71–79.
3 A. S. Hashmi and G. J. Hutchings, *Angew. Chem., Int. Ed.*, 2006, **45**, 7896–7936.
4 A. S. Hashmi and M. Rudolph, *Chem. Soc. Rev.*, 2008, **37**, 1766–1775.
5 H. Schmidbaur and A. Schier, *Chem. Soc. Rev.*, 2008, **37**, 1931–1951.
6 H. E. Abdou, A. A. Mohamed and J. P. Fackler, Jr., *Inorg. Chem.*, 2007, **46**, 9692–9699.
7 N. L. Coker, J. A. Bauer and R. C. Elder, *J. Am. Chem. Soc.*, 2004, **126**, 12–13.
8 H. Schmidbaur, *Gold Bull.*, 1990, **23**, 11–21.
9 F. Scherbaum, A. Grohmann, G. Müller and H. Schmidbaur, *Angew. Chem., Int. Ed. Engl.*, 1989, **28**, 463–465.
10 P. Pyykkö and Y. Zhao, *Angew. Chem., Int. Ed. Engl.*, 1991, **30**, 604–605.
11 M. B. Brands, J. Nitsch and C. F. Guerra, *Inorg. Chem.*, 2018, **57**, 2603–2608.
12 E. Andris, P. C. Andrikopoulos, J. Schulz, J. Turek, A. Ruzicka, J. Roithova and L. Rulisek, *J. Am. Chem. Soc.*, 2018, **140**, 2316–2325.
13 A. Lobato, M. A. Salvadó and J. M. Recio, *Chem. Sci.*, 2021, **12**, 13588–13592.
14 C. Yin, U. Wedig and M. Jansen, *Chem. Sci.*, 2021, **12**, 13593–13596.
15 A. Kovalevskiy, C. Yin, J. Nuss, U. Wedig and M. Jansen, *Chem. Sci.*, 2019, **11**, 962–969.
16 P. Pyykko, *Angew. Chem., Int. Ed.*, 2004, **43**, 4412–4456.
17 P. Schwerdtfeger, A. E. Bruce and M. R. M. Bruce, *J. Am. Chem. Soc.*, 1998, **120**, 6587–6597.
18 P. Pyykko, *Chem. Soc. Rev.*, 2008, **37**, 1967–1997.
19 P. Pyykkö, *Inorg. Chim. Acta*, 2005, **358**, 4113–4130.
20 G. J. Hutchings, M. Brust and H. Schmidbaur, *Chem. Soc. Rev.*, 2008, **37**, 1759–1765.
21 H. Schmidbaur, *Gold Bull.*, 2000, **33**, 3–10.
22 M. Jansen, *Angew. Chem., Int. Ed. Engl.*, 1987, **26**, 1098–1110.
23 M. Jansen, *J. Less-Common Met.*, 1980, **76**, 285–292.
24 H. Schmidbaur and A. Schier, *Angew. Chem., Int. Ed.*, 2015, **54**, 746–784.
25 H. Schmidbaur and A. Schier, *Organometallics*, 2015, **34**, 2048–2066.
26 S. Alvarez, *Dalton Trans.*, 2013, **42**, 8617–8636.
27 H. Schmidbaur and A. Schier, *Chem. Soc. Rev.*, 2012, **41**, 370–412.
28 C.-M. Che and S.-W. Lai, *Gold Chemistry*, 2009, pp. 249–281.
29 M. Contel, *Angew. Chem., Int. Ed.*, 2010, **49**, 250–251.
30 M. A. Omary, A. A. Mohamed, M. A. Rawashdeh-Omary and J. P. Fackler, *Coord. Chem. Rev.*, 2005, **249**, 1372–1381.
31 E. J. Fernandez, A. Laguna and J. M. Lopez-de-Luzuriaga, *Dalton Trans.*, 2007, 1969–1981.
32 V. Wing-Wah Yam, C.-K. Li and C.-L. Chan, *Angew. Chem., Int. Ed.*, 1998, **37**, 2857–2859.
33 A. L. Balch, *Angew. Chem., Int. Ed.*, 2009, **48**, 2641–2644.
34 C. K. Li, X. X. Lu, K. M. Wong, C. L. Chan, N. Zhu and V. W. Yam, *Inorg. Chem.*, 2004, **43**, 7421–7430.
35 E. C. Taylor and W. A. Ehrhart, *J. Org. Chem.*, 1963, **28**, 1108–1112.
36 K. Kaji, H. Matsubara, H. Nagashima, Y. Kikugawa and S. Yamada, *Chem. Pharm. Bull.*, 1978, **26**, 2246–2249.
37 E. C. Taylor and W. A. Ehrhart, *J. Am. Chem. Soc.*, 1960, **82**, 3138–3141.
38 D. Fenske, G. Baum, A. Zinn and K. Z. Dehnicke, *Z. Naturforsch., B: J. Chem. Sci.*, 1990, **45**, 1273–1278.
39 F. A. Cotton, X. J. Feng, M. Matusz and R. Poli, *J. Am. Chem. Soc.*, 1988, **110**, 7077–7083.
40 E. Hartmann and J. Strähle, *Z. Naturforsch., B: J. Chem. Sci.*, 1989, **44**, 1–4.
41 J. P. Coyle, P. G. Gordon, A. P. Wells, D. J. Mandia, E. R. Sirianni, G. P. A. Yap and S. T. Barry, *Chem. Mater.*, 2013, **25**, 4566–4573.
42 T. J. J. Whitehorne, J. P. Coyle, A. Mahmood, W. H. Monillas, G. P. A. Yap and S. T. Barry, *Eur. J. Inorg. Chem.*, 2011, 3240–3247.

43 H. E. Abdou, A. A. Mohamed and J. P. Fackler, *J. Cluster Sci.*, 2007, **18**, 630–641.

44 H. E. Abdou, A. A. Mohamed and J. P. Fackler, Jr., *Inorg. Chem.*, 2005, **44**, 166–168.

45 D. Y. Melgarejo, G. M. Chiarella, J. P. Fackler, Jr., L. M. Perez, A. Rodrigue-Witchel and C. Reber, *Inorg. Chem.*, 2011, **50**, 4238–4240.

46 T. J. Feuerstein, M. Poss, T. P. Seifert, S. Bestgen, C. Feldmann and P. W. Roesky, *Chem. Commun.*, 2017, **53**, 9012–9015.

47 T. J. Feuerstein, T. P. Seifert, A. P. Jung, R. Muller, S. Lebedkin, M. M. Kappes and P. W. Roesky, *Chem. – Eur. J.*, 2020, **26**, 16676–16682.

48 M. Dahlen, M. Kehry, S. Lebedkin, M. M. Kappes, W. Klopper and P. W. Roesky, *Dalton Trans.*, 2021, **50**, 13412–13420.

49 M. Dahlen, E. H. Hollesen, M. Kehry, M. T. Gamer, S. Lebedkin, D. Schooss, M. M. Kappes, W. Klopper and P. W. Roesky, *Angew. Chem., Int. Ed.*, 2021, **60**, 23365–23372.

50 M. Dahlen, N. Reinfandt, C. Jin, M. T. Gamer, K. Fink and P. W. Roesky, *Chem. – Eur. J.*, 2021, **27**, 15128–15136.

51 M. P. Coles, *Dalton Trans.*, 2006, 985–1001.

52 L. P. Hammett, *J. Am. Chem. Soc.*, 1937, **59**, 96–103.

53 L. P. Hammett, *Trans. Faraday Soc.*, 1938, **34**, 156–165.

54 J. R. Shakirova, E. V. Grachova, V. V. Gurzhiy, I. O. Koshevoy, A. S. Melnikov, O. V. Sizova, S. P. Tunik and A. Laguna, *Dalton Trans.*, 2012, **41**, 2941–2949.

55 E. M. McGarrigle, S. P. Fritz, L. Favereau, M. Yar and V. K. Aggarwal, *Org. Lett.*, 2011, **13**, 3060–3063.

56 K. E. Krahulic, G. D. Enright, M. Parvez and R. Roesler, *J. Am. Chem. Soc.*, 2005, **127**, 4142–4143.

57 A. V. Zhukhovitskiy, M. G. Mavros, T. Van Voorhis and J. A. Johnson, *J. Am. Chem. Soc.*, 2013, **135**, 7418–7421.

58 H. Kinuta, M. Tobisu and N. Chatani, *J. Am. Chem. Soc.*, 2015, **137**, 1593–1600.

59 M. Micksch, M. Tenne and T. Strassner, *Eur. J. Org. Chem.*, 2013, 6137–6145.

60 M. Cigl, A. Bubnov, M. Kašpar, F. Hampl, V. Hamplová, O. Pacherová and J. Svoboda, *J. Mater. Chem. C*, 2016, **4**, 5326–5333.

61 H. Meyer, *Monatsh. Chem.*, 1904, **25**, 1201–1214.

62 H. Nishioka, X. Liang, T. Kato and H. Asanuma, *Angew. Chem., Int. Ed.*, 2012, **51**, 1165–1168.

63 P. F. Ranken and B. G. McKinnie, *J. Org. Chem.*, 1989, **54**, 2985–2988.

64 P. J. Rayner, P. Norcott, K. M. Appleby, W. Iali, R. O. John, S. J. Hart, A. C. Whitwood and S. B. Duckett, *Nat. Commun.*, 2018, **9**, 4251.

65 C. R. Martinez and B. L. Iverson, *Chem. Sci.*, 2012, **3**, 2191–2201.

66 C. Kaub, S. Lebedkin, S. Bestgen, R. Köppe, M. M. Kappes and P. W. Roesky, *Chem. Commun.*, 2017, **53**, 9578–9581.

67 C. Kaub, S. Lebedkin, A. Li, S. V. Kruppa, P. H. Strebert, M. M. Kappes, C. Riehn and P. W. Roesky, *Chem. – Eur. J.*, 2018, **24**, 6094–6104.

68 TURBOMOLE V7.5 2020, a development of University of Karlsruhe and Forschungszentrum Karlsruhe GmbH, 1989–2007, TURBOMOLE GmbH, since 2007, available from https://www.turbomole.org.

69 J. P. Perdew, K. Burke and M. Ernzerhof, *Phys. Rev. Lett.*, 1996, **77**, 3865–3868.

70 J. P. Perdew, K. Burke and M. Ernzerhof, *Phys. Rev. Lett.*, 1997, **78**, 1396–1396.

71 S. Grimme, J. Antony, S. Ehrlich and H. Krieg, *J. Chem. Phys.*, 2010, **132**, 154104.

72 S. Grimme, S. Ehrlich and L. Goerigk, *J. Comput. Chem.*, 2011, **32**, 1456–1465.

73 X. Gui, C. Holzer and W. Klopper, *J. Chem. Theory Comput.*, 2018, **14**, 2127–2136.

74 K. Krause and W. Klopper, *J. Comput. Chem.*, 2017, **38**, 383–388.

75 A. Klamt and G. Schüürmann, *J. Chem. Soc., Perkin Trans. 2*, 1993, 799–805.